

A unifying perspective on rigidity in under-constrained materials

Matthias Merkel,¹ Karsten Baumgarten,² Brian P. Tighe,² and M. Lisa Manning¹

¹*Department of Physics, Syracuse University, Syracuse, New York 13244, USA*

²*Delft University of Technology, Process & Energy Laboratory,
Leeghwaterstraat 39, 2628 CB Delft, The Netherlands*

We present a novel approach to understanding prestress-induced rigidity in under-constrained materials, including sub-isostatic 2D spring networks and 2D and 3D vertex models for dense biological tissues. We show that in all these models a purely geometric criterion, represented by a minimal length ℓ_{\min} , determines the onset of residual stresses and rigidity. This allows us to predict not only the correct scalings for the elastic material properties, but also the precise *magnitudes* for bulk modulus and shear modulus discontinuities at the rigidity transition as well as the magnitude of the Poynting effect. We also predict from first principles that the ratio of the excess shear modulus to the shear stress should be inversely proportional to the critical strain with a prefactor of three, and propose that this factor of three is a general hallmark of prestress-induced rigidity in under-constrained materials and could be used to distinguish this effect from nonlinear mechanics of single components in experiments. Lastly, our results indicate that in many of these materials one can estimate ℓ_{\min} from measurements of local geometric structure, which in turn suggests that imaging of the network structure may be sufficient to characterize large-scale mechanical properties.

I. INTRODUCTION

A material's rigidity is intimately related to its geometry. In materials that crystallize, rigidity occurs when the constituent parts organize on a lattice. In contrast, granular systems can rigidify while remaining disordered, and arguments developed by Maxwell [1] and later refined by Calladine [2] accurately predict that the material rigidifies at an isostatic point where the number of constraints on particle motion equal the number of degrees of freedom. In both ordered and disordered systems, related theorems can be used to design materials with geometries that permit topologically protected floppy modes [3–5].

A third approach to rigidity is illustrated by a guitar string. Before it is tightened, the floppy string is under-constrained, with fewer constraints than degrees of freedom, and there are many ways to deform the string at no energetic cost. As the distance between the two ends is increased above the rest length of the string, tension (or more generally prestress or residual stress) rigidifies the system [9]. Any deformation will be associated with an energetic cost, leading to finite vibrational frequencies. This same mechanism has been proposed to be important for the elasticity of rubbers and gels [9] as well as biological cells [10].

In particular, it has been shown to rigidify under-constrained, disordered fiber networks under applied strain, with applications in biopolymer networks [11–25]. Just as with the guitar string, rigidity arises when the size and shape of the box introduce external constraints that are incompatible with the local segments of the network attaining their desired rest lengths. For example, when applying external shear, fiber networks strongly rigidify at some critical shear strain γ^* [12, 17, 19, 21–23, 25, 26], although it remains controversial whether the onset of rigidity is continuous [17, 18, 23, 27] or discontinuous [21] in the limit without fiber bending rigidity. Similarly, fiber networks can also be rigidified by isotropic dilation [13],

and the interaction between isotropic and shear elasticity in these systems is characterized an anomalous negative Poynting effect [22, 24, 28–30], i.e. the development of a tensile normal stress in response to externally applied simple shear. However, it has as yet remained unclear how all of these observations and their critical scaling behavior [12, 19, 21, 23, 31] are quantitatively connected to the underlying geometric structure of the network. Moreover, while previous works have remarked that several features of stiffening in fiber networks are surprisingly independent of model details [16], it has remained elusive whether there are generic underlying mechanisms.

Rigidity transitions have also been identified in dense biological tissues [32–36]. In particular, vertex or Voronoi models that describe tissues as a tessellation of space into polygons or polyhedra exhibit rigidity transitions [6–8, 37–49], which share similarities with both particle-based models, where the transition is driven by changes to connectivity [48], and fiber (or spring) networks, which can be rigidified by strain. Therefore, an open question is how both connectivity and strain can interact to rigidify materials [25].

Very recently, some of us showed that the 3D Voronoi model exhibits a rigidity transition driven by residual stresses [8], similar to fiber networks. Something similar has also been demonstrated for the 2D vertex model, using a continuum elasticity approach based on a local reference metric [44]. For the case of the 3D Voronoi model, we found that there was a special relationship between properties of the network geometry and the location of the rigidity transition, largely independent of the realization of the disorder [8].

Here, we show that such a relationship between rigidity and geometric structure is generic to a broad class of under-constrained materials, including spring networks and vertex/Voronoi models in different dimensions (Table I, Fig. 1). We first demonstrate that all these models display the same generic behavior in response to isotropic

TABLE I. Models discussed in this article. For the spring networks, the values indicated apply to a system size of $2N/z = 1024$ nodes, and for all cellular models values apply to a system size of $N = 512$ cells. For each model, we indicate the respective dimension d of the “length springs” and the spatial dimension D , as well as the numbers of degrees of freedom (dof) as well as constraints (i.e. length + area springs). The provided values for transition point ℓ_0^* and geometric coefficients a_ℓ , a_a , and b are average values extracted from simulations exploring the rigid regime near the transition point. For the cellular models, they are indicated together with their standard deviations across different realizations. For the 2D spring networks, the indicated numbers and their uncertainty corresponds to the respective fit of the average values with fixed exponent of Δz . Differences to earlier publications [6–8] result from differences in sampling due to a different energy minimization protocol used here (Supplemental Information, section IV).

Model	“Area” rigidity	Dim.		Number of		Transition point ℓ_0^*	Coefficients		
		d	D	dof	constr.		a_ℓ	a_a	b
2D spring network	–	1	2	$4N/z$	N	(1.506 ± 0.004) $-(0.378 \pm 0.009)\Delta z$	$(1.33 \pm 0.06)/\Delta z^{1/2}$	–	$(0.7 \pm 0.1)/\Delta z$
2D vertex	$k_A = 0$	1	2	$4N$	N	3.87 ± 0.01	0.30 ± 0.01	–	0.48 ± 0.02
2D vertex	$k_A > 0$	1	2	$4N$	$2N$	3.92 ± 0.01	1.7 ± 0.4	3.3 ± 0.7	0.6 ± 0.2
2D Voronoi	$k_A = 0$	1	2	$2N$	N	3.82 ± 0.01	0.64 ± 0.03	–	0.68 ± 0.03
3D Voronoi	$k_V = 0$	2	3	$3N$	N	5.375 ± 0.003	0.25 ± 0.01	–	0.61 ± 0.02
3D Voronoi	$k_V > 0$	2	3	$3N$	$2N$	5.406 ± 0.004	2.0 ± 0.1	6.6 ± 0.4	1.1 ± 0.1

dilation. Understanding key geometric structural properties of these systems allows us to predict the precise values of a discontinuity in the bulk modulus at the transition point. We then extend our approach to include shear deformations, which allows us to analytically predict a discontinuity in the shear modulus at the onset of rigidity. Moreover, we can make precise quantitative predictions of the values of critical shear strain γ^* , scaling behavior of the shear modulus beyond γ^* , Poynting effect, and several related critical exponents. In each case, we numerically demonstrate the validity of our approach for the case of spring networks.

We also discuss how our predictions match previously published experimental data, and highlight some new predictions, including a prefactor of three that we expect to find generically in a scaling collapse of the shear modulus, shear stress, and critical strain.

Our work connects macroscopic mechanical network properties to underlying geometric properties, which are formulated in terms of the constrained minimization of an intrinsic length $\bar{\ell}_{\min}$, and its dependence on both fluctuations and shear. This intrinsic length provides a general basis to analytically understand the strain-stiffening responses of under-constrained materials to both isotropic and anisotropic deformation within a common framework. Even though $\bar{\ell}_{\min}$ describes collective geometric effects, our work may also provide an important foundation to understand macroscopic mechanical properties from *local* geometric structure.

II. MODELS

Here we focus on four classes of models, which include 2D sub-isostatic random spring networks without bending rigidity [12, 50–54] and three models for biological tissues: the 2D vertex model [6, 37], the 2D Voronoi model

[7, 40], and the 3D Voronoi model [8] (Table I).

2D spring networks consist of nodes that are connected by in total N springs, where the average number of springs connected to a node is the coordination number z . We create networks with a defined value for z by translating jammed configurations of bidisperse disks into spring networks and then randomly pruning springs until the desired coordination number z is reached [12, 30]. We use harmonic springs, such that the total mechanical energy of the system is:

$$e_{s2D} = \sum_i (l_i - l_{0i})^2. \quad (1)$$

Here, the sum is over all springs i with length l_i and rest length l_{0i} , which are generally different for different springs. For convenience, we re-express Eq. (1) in terms of a mean spring rest length $\ell_0 = [(\sum_i l_{0i}^2)/N]^{1/2}$, which we use as a control parameter acting as a common scaling factor for all spring rest lengths. This allows us to rewrite the energy as:

$$e_{s2D} = \sum_i w_i (\ell_i - \ell_0)^2 \quad (2)$$

with rescaled spring lengths $\ell_i = \ell_0 l_i / l_{0i}$ and weights $w_i = (l_{0i} / \ell_0)^2$, such that $\sum_i w_i = N$. In simple constraint counting arguments, each spring is treated as one constraint, and here we are interested in *sub-isostatic* (i.e. under-constrained, also called *hypostatic*) networks with $z < z_c \equiv 4$.

The tissue models describe biological tissues as polygonal (2D) or polyhedral (3D) tilings of space. For the Voronoi models, these tilings are Voronoi tessellations and the degrees of freedom are the Voronoi centers of the cells. In contrast, in the 2D vertex model, the degrees of freedom are the positions of the vertices (i.e. the polygon corners). Forces between the cells are described by

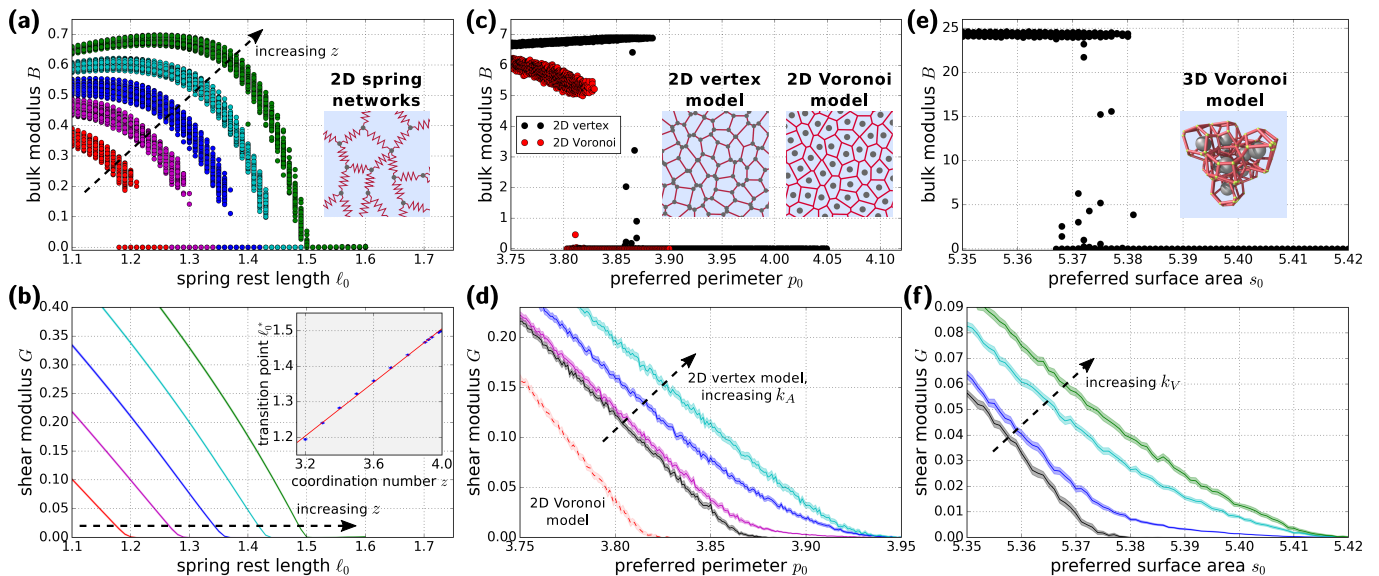


FIG. 1. Comparison of the rigidity transition across the different models: (a,b) 2D spring network (coordination numbers $z = 3.2, 3.4, 3.6, 3.8, 3.99$), (c,d) 2D Voronoi model (with $k_A = 0$) and 2D vertex model (with $k_A = 0$ in panel c and $k_A = 0, 0.1, 1, 10$ in panel d), (e,f) 3D Voronoi model (with $k_V = 0$ in panel e and $k_V = 0, 1, 10, 100$ in panel f). In all models, the transition is discontinuous in the bulk modulus (panels a,c,e) and continuous in the shear modulus (panels b,d,f). (b inset) For 2D spring networks, the value of the transition point ℓ_0^* increases with the coordination number z . This relation is approximately linear in the vicinity of the isostatic point $z_c \equiv 4$. Blue dots are simulation data and the red line shows a linear fit with $\ell_0^* = (1.506 \pm 0.004) - (0.378 \pm 0.009)\Delta z$ with $\Delta z = z_c - z$. Close to the transition point in panels c,e, data points are scattered between zero and a maximal value. This scattering is due to insufficient energy minimization in these cases. In panels b, d, and f, shaded regions indicate the standard error of the mean.

an effective energy functional. For the 2D models, the (dimensionless) energy functional is:

$$e_{c2D} = \sum_i \left[(p_i - p_0)^2 + k_A (a_i - 1)^2 \right]. \quad (3)$$

Here, the sum is over all N cells i with perimeter p_i and area a_i . There are two parameters in this model: the preferred perimeter p_0 and the relative area elasticity k_A . For the 3D Voronoi model, the energy is defined analogously:

$$e_{c3D} = \sum_i \left[(s_i - s_0)^2 + k_V (v_i - 1)^2 \right]. \quad (4)$$

The sum is again over all N cells i of the configuration, with cell surface area s_i and volume v_i , and the two parameters of the model are preferred surface area s_0 and relative volume elasticity k_V .

All four of these models are under-constrained based on simple constraint counting, as is apparent from the respective numbers of degrees of freedom and constraints listed in Table I. We stress that Calladine’s constraint counting derivation [2, 3] also applies to many-particle, non-central-force interactions.

Throughout this article, we will often discuss all four models at once. Thus, when generally talking about “elements”, we refer to springs in the spring networks and cells in the tissue models. Similarly, when talking about

“lengths ℓ ” (of dimension d), we refer to spring lengths ℓ in the spring networks, cell perimeters p in the 2D tissue models, and cell surface areas s in the 3D tissue model (Table I). Finally, when talking about “areas a ” (of dimension D), we refer to cell areas a in the 2D tissue models as well as cell volumes v in the 3D tissue model.

Here we study the behavior of local energy minima of all four models under periodic boundary conditions with fixed dimensionless system size N , i.e. the model is non-dimensionalized such that the average area per element is one [7, 8, 43]. Under these conditions, a rigidity transition exists in all models even without area rigidity. In particular, for the 2D vertex and 3D Voronoi models, we discuss the special case $k_A = 0$ separately (Table I). Moreover, the athermal 2D Voronoi model does not exhibit a rigidity transition for $k_A > 0$ [7], and thus we will only discuss the case $k_A = 0$ for this model.

III. RESULTS

A. Rigidity is created by residual stresses that are connected to a geometric criterion

We start by comparing the rigidity transitions in the four different models using Fig. 1, where we plot both the differential bulk modulus B and the differential shear modulus G versus the preferred length ℓ_0 .

In this first part, we use for all models the preferred length ℓ_0 as a control parameter. Note that because ℓ_0 is non-dimensionalized using the number density of elements, changing ℓ_0 corresponds to applying isotropic strain (i.e. a change in volume with no accompanying change in shape). Later, we will additionally include the shear strain γ as a control parameter.

In all models, we find a rigid regime ($B, G > 0$) for preferred lengths below the transition point ℓ_0^* , and a floppy regime ($B = G = 0$) above it, with the transition being discontinuous in the bulk modulus and continuous in the shear modulus. For the spring networks, we find that the transition point ℓ_0^* depends on the coordination number, where close to the isostatic point $z_c \equiv 4$, it scales linearly with the distance $\Delta z = z_c - z$ to isostaticity (Fig. 1b inset), as previously similarly discussed in [13]. Something similar has also been reported for a 2D vertex model [48].

For the cellular models, we find that the transition point for the case without area rigidity, $k_A = 0$, is generally smaller than in the case with area rigidity, $k_A > 0$ (Fig. 1d,f, Table I). Moreover, our 2D vertex model transition point for $k_A > 0$ is somewhat higher than reported before [6]. Here we used a different vertex model implementation than in [6] (Supplemental Information, section IVC), and the location of the transition in vertex models depends somewhat on the energy minimization protocol [7], a feature that is shared with other models for disordered materials [55]. Also, in Fig. 1d,f the *averaged* shear modulus always becomes zero at a higher value than the respective average transition point listed in Table I. This is due to the distribution of transition points having a finite width (see also finite width of ℓ_0 regions with both zero and nonzero bulk moduli in panels c and e).

We find that in all these models, the mechanism creating the transition is the same: rigidity is created by residual stresses through geometric incompatibility. We have already shown this for the 3D Voronoi model [8] and the 2D Voronoi model with $k_A = 0$ [7]. Our data confirms that this is the case for the 2D spring networks and the $k_A = 0$ cases of both 2D vertex and 3D Voronoi models (Supplemental Information, section IIA).

We find something similar for the 2D vertex model for $k_A > 0$. Although there are special cases where residual stresses appear in the floppy regime (Supplemental Information, section IIA), to simplify our discussion here, we only consider configurations without such typically localized residual stresses.

We observe that in all of these models, a purely geometric criterion, which we describe in terms of a minimal average length $\bar{\ell}_{\min}$, determines the onset of residual stresses. For example, in spring networks we can rewrite the energy:

$$e_{s2D} = N \left[(\bar{\ell} - \ell_0)^2 + \sigma_{\bar{\ell}}^2 \right]. \quad (5)$$

Here, $\bar{\ell} = (\sum_i w_i \ell_i) / N$ is the average of the renormalized spring length and $\sigma_{\bar{\ell}}^2 = (\sum_i w_i (\ell_i - \bar{\ell})^2) / N$ is the variance of that same quantity. Thus, energy minimization

corresponds to a simultaneous minimization with respect to $|\bar{\ell} - \ell_0|$ and $\sigma_{\bar{\ell}}$: In the floppy regime we find numerically that both quantities can vanish simultaneously and thus, all lengths attain their rest lengths, $\ell_i = \ell_0$ (Supplemental Information, section IIA). In contrast in the rigid regime, $|\bar{\ell} - \ell_0|$ and $\sigma_{\bar{\ell}}$ cannot both simultaneously vanish, creating tensions $2(\ell_i - \ell_0)$, which are sufficient to rigidify the network. The transition point ℓ_0^* corresponds to the smallest possible preferred spring length ℓ_0 for which the system can still be floppy. In other words, it corresponds to a local minimum in the average spring length $\ell_0^* = \min \bar{\ell}$ of the network under the constraint of no length fluctuations, $\sigma_{\bar{\ell}} = 0$. This defines the distribution of transition points ℓ_0^* as a purely geometric property of 2D spring networks.

For the cellular models with $k_A > 0$, we analogously find that the transition point is given by the minimal cell perimeter $\bar{\ell}$ (surface in 3D) under the constraint of no cell perimeter *and area fluctuations* $\sigma_{\bar{\ell}} = \sigma_a = 0$, which now additionally appear in the energy Eq. (5) [8]. Again, this is a purely geometric criterion, which also explains why the transition point ℓ_0^* is independent of k_A for $k_A > 0$ (Fig. 1d,f). Moreover, we can understand why the transition point is smaller for $k_A = 0$: in this case the energy does not constrain the area fluctuations, and the transition point is given by the minimal perimeter under the weaker constraint of having no perimeter fluctuations. Thus, the transition point will generally be smaller for the $k_A = 0$ case than for the $k_A > 0$ case.

B. The minimal length scales linearly with fluctuations

We next study the scaling of the minimal length in the rigid vicinity of the transition. In the rigid regime, the system must compromise between minimizing $|\bar{\ell} - \ell_0|$ and $\sigma_{\bar{\ell}}$ (and possibly σ_a in cellular models). To understand how, we must account for geometric constraints, which we express in terms of how the minimal length $\bar{\ell}_{\min} = \min \bar{\ell}$ depends on the fluctuations: $\bar{\ell}_{\min} = \bar{\ell}_{\min}(\sigma_{\bar{\ell}}, \sigma_a)$. In the rigid regime the observed average length is always greater than the preferred length, $\bar{\ell} > \ell_0$, and so the average length instead takes on its locally minimal possible value $\bar{\ell} = \bar{\ell}_{\min}(\sigma_{\bar{\ell}}, \sigma_a)$. Therefore, knowing the functional form of $\bar{\ell}_{\min}(\sigma_{\bar{\ell}}, \sigma_a)$ will allow us to predict how the system energy e (and thus also the bulk and shear moduli) depend on the control parameter ℓ_0 (Supplemental Information, section IB-D).

In section IA of the supplement, we show analytically that in the absence of residual stresses in the floppy regime, the minimal length $\bar{\ell}_{\min}$ depends linearly on the standard deviations $\sigma_{\bar{\ell}}$ and σ_a . This is directly related to the state of self-stress that is created at the onset of geometric incompatibility at $\ell_0 = \ell_0^* \equiv \bar{\ell}_{\min}(0, 0)$ [3].

To check this prediction, we numerically simulate these models, and observe indeed a linear scaling of the $\bar{\ell}_{\min}(\sigma_{\bar{\ell}})$ functions close to the transition point (Fig. 2).

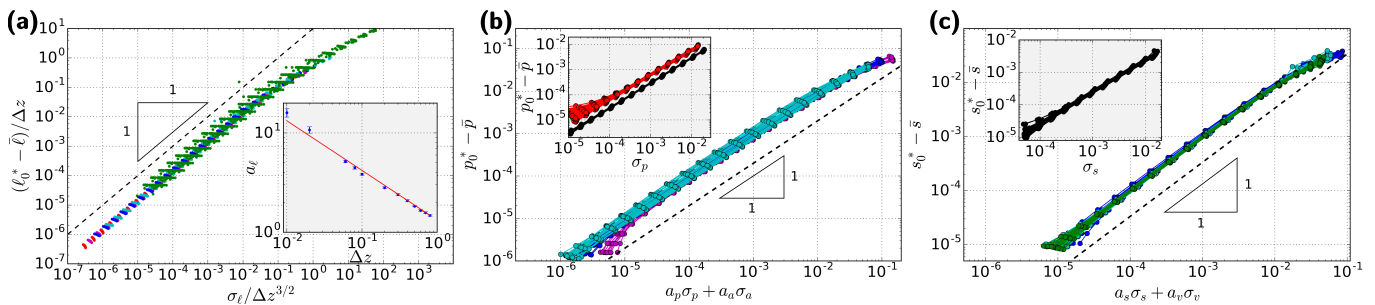


FIG. 2. Verification of the geometric linearity near the transition point. The difference between average length and transition point, $\ell_0^* - \bar{\ell}$, scales linearly with the standard deviations of lengths σ_ℓ and areas σ_a . (a) 2D spring network, (b) 2D Voronoi and vertex models, (c) 3D Voronoi model. The values of z , k_A , and k_V are respectively as in Fig. 1. (a inset) For the 2D spring networks, the coefficient a_ℓ in Eq. (6) scales with the distance to isotaticity approximately as $a_\ell \sim \Delta z^{-1/2}$.

In particular, for 2D spring networks and the $k_A = 0$ cases of the cellular models, we find:

$$\bar{\ell}_{\min}(\sigma_\ell) = \ell_0^* - a_\ell \sigma_\ell \quad (6)$$

with scaling coefficient a_ℓ . We list its value in Table I for the different models. Interestingly, we find that the coefficient a_ℓ is largely independent of the random realization of the system, in particular for cellular models with $k_A = 0$.

For 2D spring networks, a_ℓ depends on the coordination number z and approximately scales as $a_\ell \sim \Delta z^{-1/2}$ (Fig. 2a inset). This scaling behavior of a_ℓ can be rationalized using a scaling argument based on the density of states (Supplemental Information, section IE).

For cellular models where area plays a role, Eq. (6) is extended (Fig. 2b,c):

$$\bar{\ell}_{\min}(\sigma_\ell, \sigma_a) = \ell_0^* - a_\ell \sigma_\ell - a_a \sigma_a. \quad (7)$$

Again the coefficients a_ℓ and a_a are listed in Table I for 2D vertex and 3D Voronoi models. The coefficients a_ℓ differ significantly between the $k_A > 0$ and $k_A = 0$ cases of the same model, which makes sense because Eqs. (6) and (7) are linear expansions of the function $\bar{\ell}_{\min}(\sigma_\ell, \sigma_a)$ at different points (σ_ℓ, σ_a) .

C. Prediction of the bulk modulus discontinuity

Knowing the behavior of the minimal length function $\bar{\ell}_{\min}(\sigma_\ell, \sigma_a)$ in the rigid phase near the transition point provides us with an explicit expression for the energy in terms of the control parameter ℓ_0 (Supplemental Information, section IB):

$$e(\ell_0) = \frac{N}{Z} (\ell_0^* - \ell_0)^2 \quad (8)$$

with $Z = 1 + a_\ell^2 + a_a^2/k_A$, where for models without an area term the a_a^2/k_A term is dropped. Because changes in ℓ_0 correspond to changes in system size, we can predict the exact value of the bulk modulus discontinuity, ΔB ,

at the transition in all models (Fig. 1a-c, Supplemental Information, section ID):

$$\Delta B = \frac{2d^2(\ell_0^*)^2}{D^2 Z}. \quad (9)$$

This equation is for a model with d -dimensional “lengths” embedded in a D -dimensional space (see Table I). For the special case of a hexagonal lattice in the 2D vertex model, this result is consistent with Ref. [56]. More generally, for disordered networks the geometric coefficients a_ℓ and a_a appear in the denominator, because they describe non-affinities that occur in response to global isotropic deformations (Supplemental Information, section ID). A comparison of the predicted ΔB to simulation results is shown in Fig. 3.

D. Nonlinear elastic behavior under shear

As shown before [11–13, 15, 17–19, 21–24], under-constrained systems can also be rigidified by applying finite shear strain. We now incorporate shear strain γ into our formalism and test our predictions on the 2D spring networks. However, we expect our findings to equally apply to the cell-based models (Supplemental Information, section IB,C).

To extend our approach, we take into account that the minimal-length function $\bar{\ell}_{\min}(\sigma_\ell)$ can in principle also depend on the shear strain γ . We thus Taylor expand in γ :

$$\bar{\ell}_{\min}(\sigma_\ell, \gamma) = \ell_0^* - a_\ell \sigma_\ell + b\gamma^2, \quad (10)$$

where the linear term in γ is dropped due to symmetry when expanding about an isotropic state (in practice, for our finite-sized systems we drop the linear term in γ by defining the $\gamma = 0$ point using shear stabilization, Supplemental Information, sections IC and IV).

For a fixed value of γ , the interface between solid and rigid regime is again given by $\bar{\ell}_{\min}(\sigma_\ell = 0, \gamma)$, and the corresponding phase diagram in terms of both control parameters γ and ℓ_0 is illustrated in Fig. 4a. Indeed, we

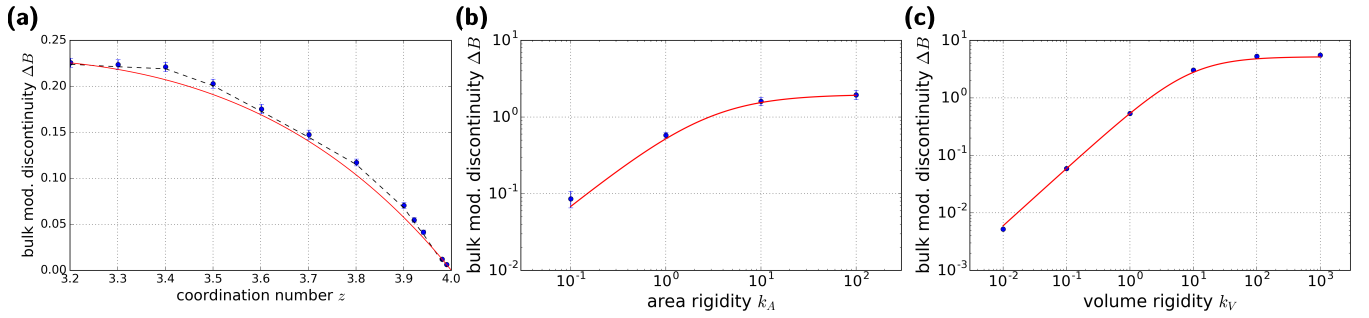


FIG. 3. Predicted and observed behavior of the bulk modulus discontinuity ΔB for (a) 2D spring networks for different values of the coordination number z , (b) the 2D vertex model for different values of the area rigidity k_A and (c) the 3D Voronoi model for different values of the volume rigidity k_V . Blue dots indicate simulations and the red curves indicate predictions without fit parameters based on Eq. (9). In panel a, the black dashed curve is computed using values for transition point ℓ_0^* and geometric scaling coefficient a_ℓ directly measured for each value of z , while for the red line we used the scaling relations from Table I.

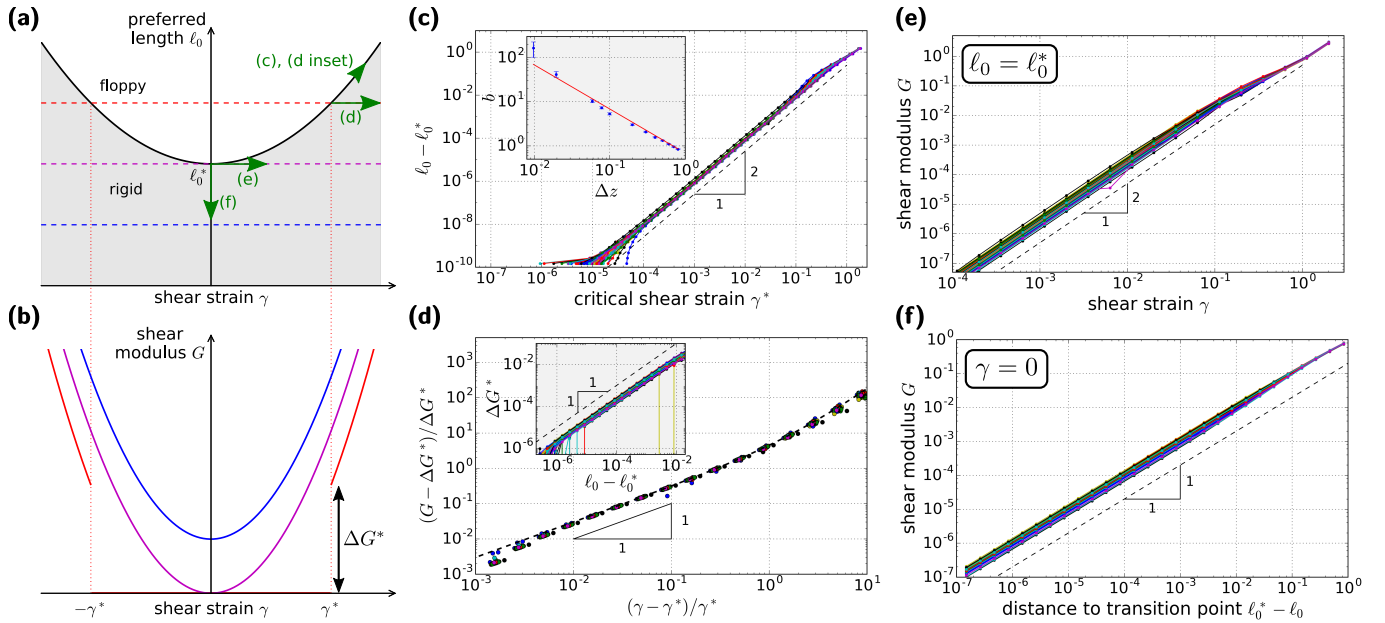


FIG. 4. Nonlinear elastic behavior of sub-isostatic spring networks under shear. (a) Schematic phase diagram illustrating the parabolic boundary between rigid (shaded) and floppy (unshaded) regime depending on preferred spring length ℓ_0 and shear strain γ . (b) Schematic showing the dependence of the shear modulus G on the shear strain γ for different values of ℓ_0 (cf. panel a). Note that for $\ell_0 > \ell_0^*$ (red curve), Eq. (12) predicts a discontinuity ΔG^* in the shear modulus at the onset of rigidity. (c) We numerically find a quadratic dependence between $\ell_0 - \ell_0^*$ and the critical shear γ^* where the network rigidifies for given $\ell_0 > \ell_0^*$. This is consistent with our Taylor expansion in Eq. (10), and the quadratic regime extends to shear strains of up to $\gamma \sim 0.1$. (c inset) The prefactor b associated with the quadratic relation in panel c scales approximately as $b \sim 1/\Delta z$. (d) Scaling of the shear modulus beyond the shear modulus discontinuity, $(G - \Delta G^*)/\Delta G^*$ over $(\gamma - \gamma^*)/\gamma^*$ with $\ell_0 - \ell_0^* = 10^{-4}$. The dashed black line indicates the prediction from Eq. (12) without fit parameters. (d inset) Scaling of the shear modulus discontinuity ΔG^* with $\ell_0 - \ell_0^*$. (e,f) Scaling of the shear modulus with γ and $\ell_0^* - \ell_0$, respectively. In all panels the coordination number is $z = 3.2$.

also numerically find a quadratic scaling for the transition line, $\ell_0 - \ell_0^* = b(\gamma^*)^2$, extending up to shear strains of $\gamma \sim 0.1$ (Fig. 4c, see also Supplemental Information, section IIB). We find that for spring networks the coefficient b depends on Δz approximately as $b \sim \Delta z^{-1}$ (Fig. 4c inset), which can be understood from properties of the density of states (Supplemental Information, section IE). To optimize precision, values of b have been

extracted from the relation $G = 4b(\bar{\ell} - \ell_0)$ in this plot (see below, cf. Fig. 4f).

Knowing the functional form of $\bar{\ell}_{\min}(\sigma_\ell, \gamma)$ close to the transition line allows us to explicitly express the energy in the rigid regime in terms of both control parameters (Supplemental Information, section IB):

$$e(\ell_0, \gamma) = \frac{N}{1 + a_\ell^2} \left(\ell_0^* - \ell_0 + b\gamma^2 \right)^2. \quad (11)$$

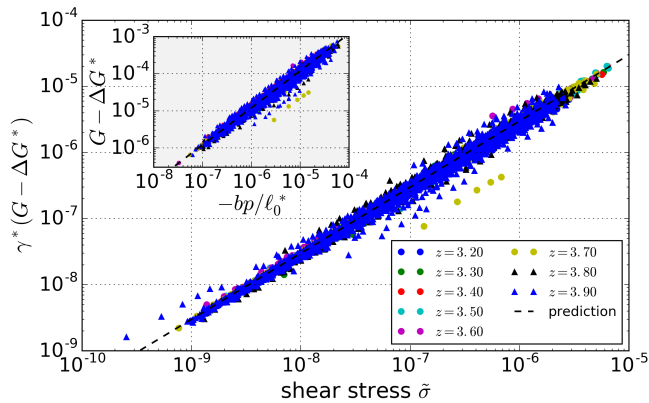


FIG. 5. The excess shear modulus $G - \Delta G^*$ scales linearly with the shear stress $\bar{\sigma}$ in 2D spring networks. We find a collapse when rescaling $G - \Delta G^*$ by the critical shear strain γ^* . The black dashed line corresponds to the prefactor of 3, as predicted by Eq. (13). (inset) The excess shear modulus $G - \Delta G^*$ scales linearly with the isotropic stress $-p$, and we obtain a collapse when rescaling the latter by b/ℓ_0^* . The black dashed line is the prediction according to Eq. (13).

This allows us to explicitly compute the shear modulus $G = (d^2e/d\gamma^2)/N$. We obtain for both floppy and rigid regime:

$$G(\ell_0, \gamma) = \Theta(\ell_0^* - \ell_0 + b\gamma^2) \frac{4b}{1 + a_\ell^2} (\ell_0^* - \ell_0 + 3b\gamma^2), \quad (12)$$

where Θ is the Heaviside function. We now discuss several consequences of this expression for the shear modulus (Fig. 4b).

When shearing the system starting in the floppy regime (i.e. for $\ell_0 > \ell_0^*$), Eq. (12) predicts a *discontinuous* change in the shear modulus of $\Delta G^* = 8b(\ell_0 - \ell_0^*)/(1 + a_\ell^2)$ at the onset of rigidity at $\gamma^* = [(\ell_0 - \ell_0^*)/b]^{1/2}$. We verify the linear scaling $\Delta G^* \sim (\ell_0 - \ell_0^*)$ in Fig. 4d inset, and the value of the scaling coefficient in the Supplemental Information, section IIB. Moreover, Eq. (12) also correctly predicts the behavior beyond γ^* , as shown in Fig. 4d.

Eq. (12) also correctly predicts the shear modulus behavior for $\ell_0 \leq \ell_0^*$. For $\ell_0 = \ell_0^*$, the shear modulus scales quadratically with γ (Fig. 4e), while for $\gamma = 0$, the shear modulus scales linearly with $(\ell_0^* - \ell_0) > 0$ (Fig. 4f, see Supplemental Information, section IC, for the cellular models), as reported before for many of the cellular models [6, 8, 56]. In both cases, we verified that the respective coefficients coincide with their expected values based on the values of a_ℓ and b .

In particular for $\gamma = 0$, because $(\ell_0^* - \ell_0) = (1 + a_\ell^2)(\bar{\ell} - \ell_0)$, we obtain the simple relation $G = 4b(\bar{\ell} - \ell_0)$, which explains the collapse in the shear modulus scaling for different k_V in the 3D Voronoi model that some of us reported earlier [8].

We also obtain explicit expressions for both shear stress $\bar{\sigma} = (de/d\gamma)/N$ and isotropic stress, i.e. negative pressure $-p$ (Supplemental Information, sections IC,D).

For the latter, we find a negative Poynting effect with coefficient $\chi \equiv p/\gamma^2 = -2db\ell_0^*/D(1 + a_\ell^2)$ at $\ell_0 = \ell_0^*$. Moreover, we find the following relations for the shear modulus:

$$G = \Delta G^* + \frac{3}{\gamma} \bar{\sigma} \quad G = \Delta G^* - \frac{6Db}{d\ell_0^*} p. \quad (13)$$

Indeed, we observe a collapse of our simulation data for the 2D spring networks in both cases (Fig. 5 & inset), where we use that close to the onset of rigidity, $\gamma \simeq \gamma^*$.

IV. DISCUSSION

In this article, we propose a unifying perspective on under-constrained materials that are stiffened by residual stresses. This is relevant for a broad class of materials [9], and has more recently been discussed in the context of biopolymer gels [11, 15–17, 24] and biological tissues [6, 8, 34, 44]. Based on generic properties of the underlying geometric structure, which we express in terms of a minimal average length function $\bar{\ell}_{\min}$, we derive the macroscopic elastic properties of a very broad class of under-constrained, prestress-rigidified materials from first principles. We numerically verify our findings using models for biopolymer networks [12, 17] and biological tissues [8, 37, 40].

Our work is relevant for experimentalists and explains the reproducibility of a number of generic mechanical features found in particular for biopolymer networks [15, 20, 24, 28]. Although strictly speaking, many biopolymer networks may not be under-constrained, it is generally assumed that their mechanics is dominated by a stretching rigidity of fibers with a sub-isostatic connectivity, which, in the absence of prestresses, is only stabilized by a weak fiber bending rigidity [15–18, 24]. For shear deformations with ℓ_0 sufficiently close to ℓ_0^* and close to the onset of rigidity $\gamma \simeq \gamma^*$, we predict a linear scaling of the differential shear modulus G with the shear stress $\bar{\sigma}$, where $(G - \Delta G^*)/\bar{\sigma} \sim 1/\gamma^*$, which has been reported before for biopolymer networks [15, 16, 24]. However, here we additionally predict from first principles that the value of the prefactor is exactly 3, largely consistent with previous experimental results [15, 24]. Moreover, our work strongly suggests that the relation $(G - \Delta G^*)/\bar{\sigma} = 3/\gamma$ is a general hallmark of prestress-induced rigidity in under-constrained materials. We thus propose it as a general experimental criterion to test whether an observed strain-stiffening behavior can be understood in terms of prestress-induced rigidity. This could help to discern e.g. whether strain-stiffening of a given biopolymer gel is due to the nonlinear mechanics of single filaments or is dominated by prestresses, a long-standing question in the field [11, 57].

We can also apply these predictions to typical rheometer geometries (Supplemental Information, section IF). We predict that an atypical tensile normal stress σ_{zz} develops under simple shear, which corresponds to a neg-

ative Poynting effect, that σ_{zz} scales linearly with shear stress and shear modulus: $\sigma_{zz} \sim \bar{\sigma} \sim (G - \Delta G^*)$ (Eq. (13) and Supplemental Information, section IF). This is precisely what has been found for many biopolymer gels like collagen, fibrin, or matrigel [15, 24, 28, 29]. However, in contrast to Ref. [24], our work suggests that the scaling factor between σ_{zz} and $(G - \Delta G^*)$ should be largely independent of γ^* . While these effects can also be explained by nonlinearities [28, 57–59], and have already been discussed in the context of prestress-induced rigidity [16, 22, 24], we show here that they represent a very generic feature of prestress-induced rigidity in under-constrained materials.

Our work also highlights the importance of isotropic deformations when studying prestress-induced rigidity, as demonstrated experimentally in Ref. [20]. While previous work [11, 12, 15, 17, 18, 21, 23, 24] focused almost [13] entirely on shear deformations, we additionally study the effect of isotropic deformations represented by the control parameter ℓ_0 . First, due to the bulk modulus discontinuity, our work predicts zero normal stress under compression and linearly increasing normal stress under expansion, consistent with experimental findings on biopolymer networks [20] (assuming the uniaxial response is dominated by the isotropic part of the stress tensor, see Supplemental Information, section IF). Second, we also correctly predict that the critical shear strain γ^* increases upon compression, which corresponds to an increase in ℓ_0 [20] (cf. Fig. 4a). While we also predict an increase of the shear modulus G under extension, which was observed as well [20], additional effects arising from the superposition of pure shear and simple shear very likely play an important role in this case. While we consider this outside the scope of this article, it will be straight forward to extend our work by this aspect.

Finally, we also provide foundations to systematically connect macroscopic mechanical material properties to the underlying *local* geometric structure. For example for collagen gels, properties of the local geometric structure can be extracted using light scattering, scanning electron microscopy, or confocal reflectance microscopy [24, 60, 61], and our work paves the way to predict how statistics of, e.g., local fiber connectivity and rest lengths affect the $\bar{\ell}_{\min}$ function and thus the elastic gel properties. Our simulations indicate that in models without area term the $\bar{\ell}_{\min}$ function does not change much when increasing system size by nearly an order of magnitude (Supplemental Information, section IIC), which suggests that local geometry may indeed be sufficient to characterize the large-scale mechanical properties of such systems.

In summary, we have developed a new approach to understand how many under-constrained disordered materials rigidify in a manner similar to a guitar string. While it is clear that the one-dimensional string becomes rigid precisely when it is stretched past its rest length, we show that in two- and three-dimensional models, rigidity is governed by a geometrical minimal length function $\bar{\ell}_{\min}$ with generic features (e.g. linear scaling with in-

trinsic fluctuations, quadratic scaling with shear strain). This insight allows us to make accurate predictions for many of the scaling functions and prefactors that describe the linear response of these materials. In addition, by performing numerical measurements of the geometry in the rigid phase to extract the coefficients of the $\bar{\ell}_{\min}$ function, we can even predict the precise magnitudes of several macroscopic mechanical properties.

In addition, these predictions help unify or clarify several scaling collapses that have been identified previously in the literature. For 2D spring networks derived from jammed packings, we studied the dependence of our geometric coefficients on the coordination number z , and find that approximately, $a_\ell \sim \Delta z^{-1/2}$ and $b \sim \Delta z^{-1}$. Combined with our finding that the value of ℓ_0 right after initialization depends linearly on z , such that $(\ell_0 - \ell_0^*) \sim \Delta z$ (data not shown), we obtain that the critical shear strain γ^* scales as $\gamma^* \sim \Delta z^\beta$ with $\beta = 1$. Similarly, we find for the associated shear modulus discontinuity $\Delta G^* \sim \Delta z^\theta$ with $\theta = 1$. While both exponents are consistent with earlier findings by Wyart et al. [12], our approach highlights the importance of the initial value of ℓ_0 for the elastic properties under shear. In other work, bond-diluted regular networks yielded different exponents β and θ [19], which is not surprising because the scaling exponents of a_ℓ and b with Δz are likely dependent on the way the network is generated. More generally, while we observed that the values of ℓ_0^* , a_ℓ , a_a , and b depended somewhat on the protocol of system preparation and energy minimization, they were relatively reproducible among different random realizations of a given protocol [55].

Moreover, we analytically predict and numerically confirm the existence and precise value of a shear modulus discontinuity ΔG^* with respect to shear deformation, whose existence for fiber networks without bending rigidity has been controversially discussed more recently [17, 18, 21, 23, 27]. We also predict a generic scaling of the shear modulus beyond this discontinuity: $(G - \Delta G^*) \sim (\gamma - \gamma^*)^f$ with $f = 1$. Smaller values for f that have been reported before for different kinds of spring and fiber networks [17, 18, 21, 23] are likely due to higher order terms in $\bar{\ell}_{\min}$. Given the very generic nature of our approach, we expect to find a value of $f = 1$ in these systems as well, if probed sufficiently close to $\ell_0 = \ell_0^*$. Note that any non-affinities, which lead to a break-down of approaches like effective medium theory close to the transition [13], are by construction fully included in our geometric coefficients a_ℓ , a_a , and b .

There are a number of possible future extensions of this work. First, we have focused here on transitions created by a minimal length, where the system is floppy for large ℓ_0 and rigid for small ℓ_0 . However, there is in principle also the possibility of a transition created by e.g. a maximal length, which is for example the case in classical sphere jamming. Although we have occasionally seen something like this in our spring networks close to isostaticity, we generally expect this to be less typical in

under-constrained systems due to buckling.

Second, while we studied here the vicinity of one local minimum of $\bar{\ell}_{\min}$ depending e.g. on γ , it would be interesting to study the behavior of the system beyond that, by including higher order terms in $\bar{\ell}_{\min}$, and by also explicitly taking plastic events into account [62]. In the case of biological tissues, plastic events typically correspond to so-called T1 transitions [63], which in our approach would correspond to changing to a different $\bar{\ell}_{\min}$ “branch”.

Third, it will be important to study what determines the exact values of the geometric coefficients a_ℓ , a_a , and b , how they depend on the network statistics, and why they are relatively reproducible. For the cellular models with area term, preliminary results suggest that the ratio of both “ a ” coefficients can be estimated by $a_a/a_\ell \approx d\ell_0^*/D$, because the self-stress that appears at the onset of rigidity seems to be dominated by a force balance between cell perimeter tension and pressure within each cell.

Fourth, because we separated geometry from energetics, it is in principle possible to generalize our work to other interaction potentials, e.g. the correct expression

for semi-flexible filaments [57, 59], and to include the effect of active stresses [54, 64, 65]. Finally, our approach can likely be extended to also include isostatic and over-constrained materials, and thus be applicable also to e.g. fiber networks with bending interactions [25].

ACKNOWLEDGMENTS

We thank Daniel M. Sussman for fruitful discussions. MM and MLM acknowledge funding from the Simons Foundation under grant number 446222, the Alfred P. Sloan Foundation, the Gordon and Betty Moore Foundation, the Research Corporation for Scientific Advancement through the Cottrell Scholars program, and computational support through NSF ACI-1541396. MLM also acknowledges support from the Simons Foundation under grant number 454947, and NSF-DMR-1352184 and NSF-PHY-1607416. KB and BPT acknowledge funding from the Netherlands Organization for Scientific Research (NWO).

-
- [1] J. C. Maxwell, *Philosophical Magazine Series 4* **27**, 294 (1864).
 - [2] C. R. Calladine, *International Journal of Solids and Structures* **14**, 161 (1978).
 - [3] T. C. Lubensky, C. L. Kane, X. Mao, A. Souslov, and K. Sun, *Reports on Progress in Physics* **78**, 73901 (2015), [arXiv:1503.01324](#).
 - [4] D. Zhou, L. Zhang, and X. Mao, *Physical Review Letters* **120**, 68003 (2018), [arXiv:1708.03935](#).
 - [5] X. Mao and T. C. Lubensky, *Annu. Rev. Condens. Matter Phys* **9**, 413 (2018).
 - [6] D. Bi, J. H. Lopez, J. M. Schwarz, and M. L. Manning, *Nature Physics* **11**, 1074 (2015), [arXiv:1409.0593](#).
 - [7] D. M. Sussman and M. Merkel, *Soft Matter* (2018), [10.1039/C7SM02127E](#), [arXiv:1708.03396](#).
 - [8] M. Merkel and M. L. Manning, *New Journal of Physics* **20**, 022002 (2018).
 - [9] S. Alexander, *Physics Report* **296**, 65 (1998), [arXiv:1512.04885](#).
 - [10] D. E. Ingber, N. Wang, and D. Stamenović, *Reports on Progress in Physics* **77**, 046603 (2014), [arXiv:NIHMS150003](#).
 - [11] P. R. Onck, T. Koeman, T. van Dillen, and E. van der Giessen, *Physical Review Letters* **95**, 178102 (2005), [arXiv:0502397 \[cond-mat\]](#).
 - [12] M. Wyart, H. Liang, A. Kabla, and L. Mahadevan, *Physical Review Letters* **101**, 1 (2008), [arXiv:0806.4571v1](#).
 - [13] M. Sheinman, C. P. Broedersz, and F. C. MacKintosh, *Physical Review E* **85**, 021801 (2012), [arXiv:1108.3981](#).
 - [14] J. L. Silverberg, A. R. Barrett, M. Das, P. B. Petersen, L. J. Bonassar, and I. Cohen, *Biophysical Journal* **107**, 1721 (2014).
 - [15] A. J. Licup, S. Münster, A. Sharma, M. Sheinman, L. M. Jawerth, B. Fabry, D. a. Weitz, and F. C. MacKintosh, *Proceedings of the National Academy of Sciences* **112**, 9573 (2015), [arXiv:1503.00924](#).
 - [16] A. J. Licup, A. Sharma, and F. C. MacKintosh, *Physical Review E* **93**, 012407 (2016).
 - [17] A. Sharma, A. J. Licup, K. A. Jansen, R. Rens, M. Sheinman, G. H. Koenderink, and F. C. MacKintosh, *Nature Physics* **12**, 584 (2016), [arXiv:1506.07792](#).
 - [18] A. Sharma, A. J. Licup, R. Rens, M. Vahabi, K. A. Jansen, G. H. Koenderink, and F. C. MacKintosh, *Physical Review E* **94**, 042407 (2016), [arXiv:1606.08218](#).
 - [19] J. Feng, H. Levine, X. Mao, and L. M. Sander, *Soft Matter* **12**, 1419 (2016).
 - [20] A. S. G. van Oosten, M. Vahabi, A. J. Licup, A. Sharma, P. A. Galie, F. C. MacKintosh, and P. A. Janmey, *Scientific Reports* **6**, 19270 (2016).
 - [21] M. F. J. Vermeulen, A. Bose, C. Storm, and W. G. Ellenbroek, *Physical Review E* **96**, 053003 (2017), [arXiv:1709.02622](#).
 - [22] J. Shivers, J. Feng, A. Sharma, and F. C. MacKintosh, [arXiv:1711.00522](#) (2017).
 - [23] J. Shivers, S. Arzash, A. Sharma, and F. C. MacKintosh, [arXiv:1807.01205](#) (2018).
 - [24] K. A. Jansen, A. J. Licup, A. Sharma, R. Rens, F. C. MacKintosh, and G. H. Koenderink, *Biophysical Journal* **114**, 2665 (2018).
 - [25] R. Rens, C. Villarroel, G. Düring, and E. Lerner, [arXiv:1808.04756](#) (2018).
 - [26] S. Rammensee, P. A. Janmey, and A. R. Bausch, *European Biophysics Journal* **36**, 661 (2007).
 - [27] R. Rens, M. Vahabi, A. J. Licup, F. C. MacKintosh, and A. Sharma, *The Journal of Physical Chemistry B* **120**, 5831 (2016).
 - [28] P. A. Janmey, M. E. McCormick, S. Rammensee, J. L. Leight, P. C. Georges, and F. C. MacKintosh, *Nature Materials* **6**, 48 (2007).
 - [29] H. C. G. de Cagny, B. E. Vos, M. Vahabi, N. A. Kurni-

- awan, M. Doi, G. H. Koenderink, F. C. MacKintosh, and D. Bonn, *Physical Review Letters* **117**, 217802 (2016).
- [30] K. Baumgarten and B. P. Tighe, *Physical Review Letters* **120**, 148004 (2018).
- [31] C. P. Broedersz, X. Mao, T. C. Lubensky, and F. C. MacKintosh, *Nature Physics* **7**, 983 (2011).
- [32] T. E. Angelini, E. Hannezo, X. Trepap, M. Marquez, J. J. Fredberg, and D. a. Weitz, *Proceedings of the National Academy of Sciences* **108**, 4714 (2011).
- [33] M. Sadati, N. Taheri Qazvini, R. Krishnan, C. Y. Park, and J. J. Fredberg, *Differentiation* **86**, 121 (2013).
- [34] J.-A. Park, J. H. Kim, D. Bi, J. A. Mitchel, N. T. Qazvini, K. Tantisira, C. Y. Park, M. McGill, S.-H. Kim, B. Gweon, J. Notbohm, R. Steward Jr, S. Burger, S. H. Randell, A. T. Kho, D. T. Tambe, C. Hardin, S. A. Shore, E. Israel, D. A. Weitz, D. J. Tschumperlin, E. P. Henske, S. T. Weiss, M. L. Manning, J. P. Butler, J. M. Drazen, and J. J. Fredberg, *Nature Materials* **14**, 1040 (2015).
- [35] S. Garcia, E. Hannezo, J. Elgeti, J.-F. Joanny, P. Silberzan, and N. S. Gov, *Proceedings of the National Academy of Sciences* **112**, 15314 (2015).
- [36] C. Malinverno, S. Corallino, F. Giavazzi, M. Bergert, Q. Li, M. Leoni, A. Disanza, E. Frittoli, A. Oldani, E. Martini, T. Lendenmann, G. Deflorian, G. V. Beznoussenko, D. Poulidakos, K. H. Ong, M. Uroz, X. Trepap, D. Parazzoli, P. Maiuri, W. Yu, A. Ferrari, R. Cerbino, and G. Scita, *Nature Materials* **16**, 587 (2017).
- [37] R. Farhadifar, J. C. Röper, B. Aigouy, S. Eaton, and F. Jülicher, *Current Biology* **17**, 2095 (2007), [arXiv:1112.5905v1](#).
- [38] D. B. Staple, R. Farhadifar, J. C. Röper, B. Aigouy, S. Eaton, and F. Jülicher, *The European Physical Journal E* **33**, 117 (2010).
- [39] D. Bi, J. H. Lopez, J. M. Schwarz, and M. L. Manning, *Soft Matter* **10**, 1885 (2014), [arXiv:1308.3891](#).
- [40] D. Bi, X. Yang, M. C. Marchetti, and M. L. Manning, *Physical Review X* **6**, 021011 (2016).
- [41] D. A. Matoz-Fernandez, K. Martens, R. Sknepnek, J. L. Barrat, and S. Henkes, *Soft Matter* **13**, 3205 (2017), [arXiv:1610.09340](#).
- [42] D. L. Barton, S. Henkes, C. J. Weijer, and R. Sknepnek, *PLOS Computational Biology* **13**, e1005569 (2017), [arXiv:1612.05960](#).
- [43] X. Yang, D. Bi, M. Czajkowski, M. Merkel, M. L. Manning, and M. C. Marchetti, *Proceedings of the National Academy of Sciences* **114**, 12663 (2017), [arXiv:1704.05951](#).
- [44] M. Moshe, M. J. Bowick, and M. C. Marchetti, *Physical Review Letters* **120**, 268105 (2017), [arXiv:1708.07848](#).
- [45] F. Giavazzi, M. Paoluzzi, M. Macchi, D. Bi, G. Scita, L. Manning, R. Cerbino, and M. C. Marchetti, *Soft Matter* (2018), [10.1039/C8SM00126J](#), [arXiv:1706.01113](#).
- [46] D. M. Sussman, M. Paoluzzi, M. Cristina Marchetti, and M. Lisa Manning, *EPL (Europhysics Letters)* **121**, 36001 (2018), [arXiv:1712.05758](#).
- [47] A. Boromand, A. Signoriello, F. Ye, C. S. O'Hern, and M. Shattuk, [arXiv:1801.06150](#) (2018).
- [48] L. Yan and D. Bi, [arXiv:1806.04388](#) (2018).
- [49] E. Teomy, D. A. Kessler, and H. Levine, [arXiv:1803.03962](#) (2018).
- [50] B. P. Tighe, *Physical Review Letters* **109**, 168303 (2012).
- [51] M. Yucht, M. Sheinman, and C. Broedersz, *Soft Matter* **9**, 7000 (2013).
- [52] G. Düring, E. Lerner, and M. Wyart, *Soft Matter* **9**, 146 (2013), [arXiv:1204.3542](#).
- [53] G. Düring, E. Lerner, and M. Wyart, *Physical Review E* **89**, 022305 (2014).
- [54] F. G. Woodhouse, H. Ronellenfitch, and J. Dunkel, [arXiv:1805.07728](#) (2018).
- [55] P. Chaudhuri, L. Berthier, and S. Sastry, *Physical Review Letters* **104**, 165701 (2010), [arXiv:0910.0364](#).
- [56] N. Murisic, V. Hakim, I. G. Kevrekidis, S. Y. Shvartsman, and B. Audoly, *Biophysical Journal* **109**, 154 (2015).
- [57] C. Storm, J. J. Pastore, F. C. MacKintosh, T. C. Lubensky, and P. A. Janmey, *Nature* **435**, 191 (2005).
- [58] H. Kang, Q. Wen, P. A. Janmey, J. X. Tang, E. Conti, and F. C. MacKintosh, *The Journal of Physical Chemistry B* **113**, 3799 (2009).
- [59] A. R. Cioroianu and C. Storm, *Physical Review E* **88**, 052601 (2013).
- [60] B. A. Roeder, K. Kokini, J. E. Sturgis, J. P. Robinson, and S. L. Voytik-Harbin, *Journal of Biomechanical Engineering* **124**, 214 (2002), [arXiv:9809069v1](#) [[arXiv:gr-qc](#)].
- [61] S. B. Lindström, D. A. Vader, A. Kulachenko, and D. A. Weitz, *Physical Review E* **82**, 051905 (2010).
- [62] H. Amuasi, A. Fischer, A. Zippelius, and C. Heussinger, [arXiv:1808.05407](#) (2018).
- [63] S. Kim, Y. Wang, and S. Hilgenfeldt, *Physical Review Letters* **120**, 248001 (2018).
- [64] S. Stam, S. L. Freedman, S. Banerjee, K. L. Weirich, A. R. Dinner, and M. L. Gardel, *Proceedings of the National Academy of Sciences* **114**, E10037 (2017).
- [65] E. Fischer-Friedrich, *Biophysical Journal* **114**, 419 (2018).